Journal of Computational Physics 228 (2009) 2690–2706

Contents lists available at ScienceDirect

Journal of Computational Physics

journal homepage: www.elsevier.com/locate/jcp

Letter to the editor

A triple level finite element method for large eddy simulations

Weiming Liu *

Centre for Research in Fire and Explosion Studies, University of Central Lancashire, Preston PR1 2HE, UK

ARTICLE INFO

Article history:
Received 3 March 2008
Received in revised form 21 November 2008
Accepted 9 December 2008
Available online 24 December 2008

Keywords:
Turbulence
Large eddy simulation
Multiscale finite element method
Implicit LES

ABSTRACT

Since large eddy simulation (LES) was introduced by Smagorinsky in 1963, it has been improved with various thoughts from many researchers. Unfortunately, despite that, the filtered approach that is widely used at present still suffers because quite empirical factors are used to determine non-closured subgrid Reynolds stresses. Based on a new definition of LES and multiscale finite element concepts, this work presents an attempt to remove such factors. Using direct sum decomposition of the solution space, we devised a hierarchical multi-level formulation of the Navier–Stokes equations for turbulence. The base-level, bearing the information of large eddies, is calculated by the conventional finite element method. The finer levels are for small scale eddies of turbulence. We address the solution methods for the small scale movements. In particular, a spectral element method is introduced for the finer level solutions. Thus large eddies and small eddies to some extent may be accurately obtained. The introduced approach offers not only access to calculate turbulence in complex geometries because of the nature of finite element method but also an effective tool for multiscale physical problems with turbulence, such as reaction flows. It is worth noting that the approach introduced here is similar to the implicit LES in finite volume and finite difference methods.

1. Introduction

Solving the filtered Navier–Stokes equations is a major approach for large eddy simulation (LES) of turbulence at present. Unfortunately, this approach leads to great difficulty to accurately calculate the unclosed subgrid Reynolds stresses produced by this filtered method when applied to turbulence simulations of complex geometry, since the widely used viscosity model is, in fact, inadequate for determining the subgrid Reynolds stresses in many cases [3]. There have been several attempts to overcome the difficulty, for example, inertial manifold concept and non-linear Galerkin methods [6,12,13,32,33], implicit LES [1,4,10,19,28,36] and variational multiscale methods for LES [3,17,18,23,24]. Of these works, it seems that the variational multiscale methods for LES are more practical and provide possible routes to the solution of turbulence modelling problem in complex geometries. This is because this approach (1) is capable of providing a solid mathematic foundation on which the various-scale turbulent movements can be reasonably and accurately approximated; (2) dispels the commutativity restriction of unstructured meshes, as a consequence, may be implemented in complex geometries without difficulty; and (3) ensures stability of algorithms and supplies a favourable numerical attribute for computational performances, such as convergence etc.

Although there is such potential advantage, most of the previous works employing variational multiscale methods remained under the framework of the filtered approach and were not extricated from eddy viscosity modelling, however recently a work published [3] tries to calculate the small scale movement of turbulence without the Smagorinsky – like viscosity models.

* Tel.: +44 1772 893239.
E-mail address: wliul@uclan.ac.uk

0021-9991/$ - see front matter © 2008 Elsevier Inc. All rights reserved.
doi:10.1016/j.jcp.2008.12.004

The aim of this work, like [3], is to remove the inaccurate viscosity models from LES. First of all, we introduce a new definition of LES. Under the new definition, a hierarchical multi-level formulation of the Navier–Stokes equations for LES is derived, based on the concepts of direct sum decomposition of the solution space and multiscale finite elements. We then address the strategies required to solve the turbulent movements of each level. In particular, we give an algorithm for triple level solutions. That is, the solution for the first level is calculated by the conventional finite method; the one for the second level by the spectral element method and the one for last level (finest level) by the analytic expressions that approximate the solution of the sub-problems on this level. Recently, several three-level schemes have been proposed, see [9,16–18,30]. However, this work may be the first for the combination of the traditional finite element method and spectral element method to compute LES and, in the author's view, such a combination may gain a better trade-off between accurate results and computational cost.

2. Formulations

We consider incompressible viscous flows in this work. Nevertheless it should be noted that the introduced approach is not only confined to the incompressible flows, but may easily be extended to the other flows, e.g. low Mach thermal flows with reactions, as well. The incompressible viscous flow of a fluid is governed by the Navier–Stokes equations:

$$\nabla \cdot \vec{u} = 0, \quad \text{on} \quad \Omega \times (0,T) \tag{1}$$

$$\rho \frac{\partial \vec{u}}{\partial t} + \rho(\vec{u} \cdot \nabla)\vec{u} + \nabla p - \eta \nabla \cdot \pi = 0, \quad \text{on} \quad \Omega \times [0,T] \tag{2}$$

where Ω and $[0,T]$ are a spatial and temporal domain, and $x \in \bar{\Omega}$ (the set closure of the spatial domain) and $t \in [0,T]$ are the associated coordinates. The unknowns, $\vec{u}$ and p, denote the flow velocity vector and pressure, respectively. The parameters, η and ρ, are respectively the viscosity and the density of fluid, which are taken as constant in this work. The variable, $\pi = \nabla\vec{u} + (\nabla\vec{u})^T$, is the strain tensor of the flow velocities and has a relation with the stress tensor, σ, occurring in Eq. (4), $\sigma = \eta\pi$.

The initial conditions are defined by the velocity distributions at the initial time instant and have the following general form:

$$\vec{u} = \vec{u}(x) \quad \text{on} \quad \bar{\Omega} \tag{3}$$

In this work, we consider the boundary conditions of these types

$$\vec{u} = \vec{f}, \text{on } \Gamma_1, -\vec{n}p + \vec{n} \cdot \sigma = \vec{g} \quad \text{on} \quad \Gamma_2 \tag{4}$$

where $\Gamma = \Gamma_1 \cup \Gamma_2$ and σ denote the boundary surfaces of the flow domain and the shear stress tensor of the fluid, respectively. The functions $\vec{f}$ and $\vec{g}$ in Eq. (4) are prescribed, and $\vec{n}$ are the unit normal vector of the flow domain, respectively. This is a typical initial-boundary value problem for incompressible flows. It is widely used in practice.

2.1. Hierarchical multi-level formulation for LES

The Navier–Stokes problem (1)–(4) will become unstable and turbulent when Reynolds number exceeds a critical condition. Turbulence is characterised by random fluctuation with a wide range of frequency which generally depends upon Reynolds number. An accurate numerical solution of the Navier–Stokes problem for turbulence should cover the whole frequency scale. This requires a very fine computational mesh and time step, and therefore is often impracticable in applications. An approximate strategy to replace this is large eddy simulation (LES). In concept, LES is a solution such that it retains major energy or eddies of turbulence but removes small fluctuation which is normally distributed in the high frequency range. In this section we derive a new hierarchical multi-level formulation of finite element method for LES.

The weak solution in Galerkin sense of the problem (1)–(4) reads:

$$\int_\Omega \vec{v} \cdot \rho\left(\frac{\partial \vec{u}}{\partial t} + \vec{u} \cdot \nabla \vec{u}\right) d\Omega - \int_\Omega \nabla \vec{v} \cdot p d\Omega + \eta \int_\Omega \nabla \vec{v} : \pi d\Omega + \int_\Omega q \nabla \cdot \vec{u} d\Omega = \int_{\Gamma_2} \vec{v} \cdot (\vec{g} \cdot \vec{n}) d\Gamma \tag{5}$$

where $\vec{u} \in H^u(\Omega)$, $\vec{v} \in H_0^u(\Omega)$, $p \in H^p(\Omega)$ and $q \in H_0^p(\Omega)$; $H^u(\Omega)$ and $H^p(\Omega)$ are the $L^2(\Omega)$ based Sobolev spaces with norm $\|\vec{u}\|_{1,\Omega} = \left(\int_\Omega \sum_{|k|\leqslant 1} |D^k \vec{u}|^2\right)^{\frac{1}{2}}$ and $\|p\|_{1,\Omega} = \left(\int_\Omega \sum_{|k|\leqslant 1} |D^k p|^2\right)^{\frac{1}{2}}$, and seminorms, $|\vec{u}|_{1,\Omega} = \left(\int_\Omega \sum_{|k|=1} |D^k \vec{u}|^2\right)^{\frac{1}{2}}$ and $|p|_{1,\Omega} = \left(\int_\Omega \sum_{|k|=1} |D^k p|^2\right)^{\frac{1}{2}}$, respectively; and $H_0^u(\Omega)$ and $H_0^p(\Omega)$ are the closed subset of $H^u(\Omega)$ and $H^u(\Omega)$, respectively, which vanish on $\partial\Omega$. For numerical solution purposes, Eq. (5) is linearized by the Newton method. In the linearized step, the velocities before the gradient operator of the convective term are viewed as constant. Having a solution of the linearized problem we carry out Newton iterations until convergence of the non-linear problem. During the Newton iterations the constant velocities in the linear step will be updated by their linear solution from the previous iterations. Hence, the following context will mainly focus on the solution of the linearized problem of (5).

Before further developing the numerical solution let us introduce an operator for (1) and (2):

$$L = \begin{pmatrix} \rho\frac{\partial}{\partial t} + \rho\vec{u}\cdot\nabla - \eta(\nabla^2) & \nabla \\ \nabla\cdot & 0 \end{pmatrix} \tag{6}$$

Using this operator, Eqs. (1) and (2) may be rewritten as

$$L(S) \equiv L\begin{pmatrix} \vec{u} \\ p \end{pmatrix} = F \equiv \begin{pmatrix} 0 \\ 0 \end{pmatrix} \tag{7}$$

Consider an approximation of the solution space of the problem (5). It is a direct sum decomposition of two spaces

$$U = U^h \oplus U^b \tag{8}$$

where $U^h = \begin{pmatrix} U_u^{3h}, & U_p^h \end{pmatrix}$ is the trial function spaces of the standard finite element method, which are in this work defined as

$$U_u^{3h} = \{\vec{u}^h | \vec{u}^h \in H^{3h}, \vec{u}^h = \vec{f}, \quad \text{on} \quad \Gamma_1\} \tag{9}$$

$$U_p^h = \{p^h | p^h \in H^{1h}\} \tag{10}$$

where $H^{1h} = H^h$ and $H^{3h} = \{H^h \times H^h \times H^h\}$. Here H^h is defined as $H^h = \{\varphi^h | \varphi^h \in C^0(\bar{\Omega}), \varphi^h|_{\Omega_e} \in P^1, \forall \Omega_e \in D\}$, and P^1 denotes the first order polynomials and D the set of the finite element discretization of the domain Ω. This means that equal-order trilinear interpolation function space is used for the hexahedral element and/or linear interpolation function space for the tetrahedral element. The velocity and pressure are arranged on collocated mesh nodes.

The space U^h has finite dimensions. It is expected to bear the information of large eddies of turbulence. How fine the scale eddies the numerical solution can represent depends on the dimensions of this space (or mesh resolution), time step width and applied numerical scheme. The Nyquist–Shannon sampling theorem states the limitation of the resolution of computational mesh and time step width for representation of small scale eddy. When considering finer eddies, we should be aware of this limitation of computational mesh resolution and time step width. Now we define that *a large eddy simulation of turbulence on this space U^h is the sample having the exact solution of the turbulence at a particular time instant at mesh nodes* or *, an equivalent form, is the projection of the time series of the exact solution onto the space U^h*.[1] This definition, in form, is different from the LES definition with the traditional filter but it substantially accords with the spirit of LES. The detailed discussion of this issue may be seen in [25]. Based on this definition our major intent is to design such a numerical scheme for Eq. (5) so as to ensure that the values of the velocity and pressure on the computational mesh approach to the exact solution as closely as possible in an implementable range.

When we directly project Eq. (5) onto the space U^h by the traditional finite element method, the numerical solution would not only lead to a large truncation error which misses too much information about turbulent eddies but also produce serious numerical instabilities.[2] In fact, the numerical instabilities are caused by the truncation error, see [22,26]. As a consequence, our numerical scheme to be derived is to capture the effects of the small scale eddies which are simply abandoned on the space U^h by the traditional finite element method. When the abandoned small scale movements are successfully captured, we may both gain more accurate solution information on the large eddies and eliminate the numerical instabilities. Coincidentally, the original motivation of Smagorinsky to introduce LES and the subgrid Reynolds stress was for the purpose of stabilising numerical computation while preserving accuracy of the small scale movement [31]. This motivation is retained with this work but we take a different route for implementation.

In order to capture the small scale eddies, let us enlarge the space U^h by a subspace U^b which carries on the small scale movement. There are different choices for the subspace U^b. Each scheme necessarily impacts on the computational accuracy, the complexity of implementation of the method and the requirement of computer resource. One option is the bubble function space on the element, $U^b = \oplus_e U_e^B$ and U_e^B is the space of bubble in the element, E. This means that the values of functions from the subspaces vanish on the element boundary, i.e., $U_e^B = (H_0^u(E), H_0^p(E))$.

Having the subspace U^b, Galerkin formulation (5) is projected onto the two decomposed spaces (8)

$$(L(S), v^h) \equiv (L(S^h), v^h) + (L(S^b), v^h) = (F, v^h) \quad v^h \in V^h \tag{11}$$

$$(L(S), v_b^h) \equiv (L(S^h), v_b^h) + (L(S^b), v_b^h) = (F, v_b^h) \quad v_b^h \in U^b \tag{12}$$

where $S = S^h + S^b \in U (S^h \in U^h, S^b \in U^b)$ and the test function spaces, $V^h = \begin{pmatrix} V_v^h, & V_p^h \end{pmatrix}$, is defined as

$$V_v^h = \left\{ v^h | v^h \in H^{3h}, v^h = 0, \quad \text{on} \quad \Gamma_1 \right\} \tag{13}$$

$$V_q^h = \left\{ q^h | q^h \in H^{1h} \right\} \tag{14}$$

[1] Note that the interpolation function of finite element space has the property $H_i(x) = \begin{cases} 1, & x = x_i \\ 0, & x = x_j \ (i \neq j) \end{cases}$, where x_j is the node of the mesh.

[2] Two famous instabilities in the incompressible flows: convective instability and saddle point problem's instability.

Due to the property of the bubble function space, Eq. (12) is actually a weak solution of the following problem

$$\begin{cases} L(S^b) = -\{L(S^h) - F\} & \text{in } E \\ S^b = 0 & \text{on } \partial E \end{cases} \tag{15}$$

Eq. (15) presents a basic problem for the small scale eddies on each element, and it makes the solution for the small scale movement localised, i.e., independent of the other elements, and therefore reduces the computational cost significantly. The right hand side term of Eq. (15) $-\{L(S^h) - F\}$, is the residual of the traditional Galerkin finite element projection. It is like the truncation error produced due to finite dimensions of the space U^h, and this term supplies the energy to maintain the small eddies.

Integrating by parts the second term on the left hand side of (11) and also considering the property of the bubble function subspace, we have

$$(L(S^b), v^h) = (S^b, L^*(v^h)) \tag{16}$$

where L^* is the formal adjoint of L on E. If we use L^{-1} to denote the negative inverse of the operator defined by (15) and consider Eq. (16), then Eq. (11) can be rewritten as

$$(L(S^h), v^h) + (L^{-1}(L(S^h) - F), L^*(v^h)) = (F, v^h) \tag{17}$$

The second term of Eq. (17) on the left hand side shows the effect of the small scale on the large eddy, i.e., the small scale movement to be captured. This term plays an important role in stabilising the algorithm as well. Due to linear interpolation function on each element,$L(S^h) - F$ and $L^*(v^h)$ are constant in each element E. As a result, Eq. (17) can be reduced into

$$(L(S^h), v^h) + (\tau \cdot (L(S^h) - F), L^*(v^h)) = (F, v^h) \tag{18}$$

where $\tau = \frac{1}{|E|}\int_E L^{-1}(1)dE = \frac{1}{|E|}\int_E b_E dE$ is a vector parameter, and b_E is a solution of the following problem in E

$$\begin{cases} L(b_E) = 1 & \text{in } E \\ b_E = 0 & \text{on } \partial E \end{cases} \tag{19}$$

A similar derivation of Eq. (19) can be seen in [5] and [27], which give more detail.

Up to now, using the assumption of the bubble function subspace, we have derived the basic equations for large and small eddies of turbulence, (18) and (15) or (19). The problem (18) is a conventional finite element problem, when the small scale eddies are known and therefore will be easily resolved, while the problem (15) or (19) remains an infinite dimensional problem. How to solve it will be discussed in the following sections. The parameter τ represents the integral effect of the small scale movement on the large eddy. In form it is similar to the eddy viscosity of the viscosity model. However, there are significant differences between the two approaches: (1) the parameter τ enhances stability of numerical computations, so does the eddy viscosity; (2) the parameter τ results in more accurate numerical solutions since it is obtained through extending the solution space, this is not the case for the eddy viscosity; (3) the parameter τ is computable from problem (15) or (19), but the eddy viscosity is not.

The problem (15) or (19) can now be seen as a particular example of problem (1)–(4) on an element domain which can be solved in different ways that generally depend on the requirement of physical problem and the mesh resolution or grid Reynolds number. In this work we discuss two approaches:

(a) When the grid Reynolds number is small the solution on the solution level already includes major turbulent energy, and the turbulent energy of upper level flows may be assumed to be minor. Thus we can use the known approximate solutions of problem (15) or (19) for laminar flows proposed by some researchers as the parameter τ. Here are given three approximate formulations
The first is from [15]

$$\begin{cases} \tau_u = \frac{h}{2\|u^h\|}\zeta(\mathrm{Re}^u) \\ \tau_p = 0 \end{cases} \tag{20}$$

The second is proposed by [35]

$$\begin{cases} \tau_u = \frac{h}{2\|u^h\|}\zeta(\mathrm{Re}^u) \\ \tau_p = \lambda\|u^h\|h\zeta(\mathrm{Re}^u) \end{cases} \tag{21}$$

The last is suggested by [8]

$$\begin{cases} \tau_u = \left[\left(c_1\frac{\|u^h\|}{h}\right)^2 + \left(c_2\frac{v}{h^2}\right)^2\right]^{-\frac{1}{2}} \\ \tau_p = c_2\frac{h^2}{\tau_u} \end{cases} \tag{22}$$

where h and u^h denote the element length and local velocity, respectively. $Re^u$is the element Reynolds number, and c_1 and c_2 are two constants. The function,$\zeta(x)$, is defined as

$$\zeta(x) = \begin{cases} \frac{x}{3}, & 0 \leqslant x \leqslant 3 \\ 1, & 3 \leqslant x \end{cases} \tag{23}$$

(b) When the grid Reynolds number is not small, the computational method described in section (a) would lead to a large error, hence we need to refine the element solution of problem (15) or (19). Firstly we do a direct sum decomposition of the bubble subspace S^b as (24), then project problem (15) or (19) onto such decompositions, which in form are almost the same as (18) and (15) or (19)

$$S^b = S^h_{e\_b} \oplus S^b_{e\_b} \tag{24}$$

The solution of the problem projected on the space $S^h_{e\_b}$ represents turbulence on level two which will be used to compute the integration for the parameter τ of Eq. (18). If $S^h_{e\_b} \in U^h$ (the same trial function space as one for (18)), the decomposition (18) leads to an h – type refinement and implementation of this refinement is straightforward and we shall not discuss this case in this work; else if $S^h_{e\_b} \in U^h_n$ (a trial function space consisting of n – order polynomials), then the decomposition (24) results in a p – type refinement. Section 2.1 will explain how to implement this refinement by spectral element method.

The subspace $S^b_{e\_b}$ is a new bubble function space on the refined element, therefore the solution of the problem projected on it is of smaller turbulent energy, as a consequence, it is calculated by the approximate methods given in the section (a).

We may repeatedly carry out the same procedure of derivation as the section (b) when needed. In this way a hierarchical structure of multi-level formulation for the problem (5) is obtained. This hierarchical formulation, in fact, is a series of approximations to the infinite dimensional space, and it provides a theoretical framework to calculate the multi-scale physical problem of turbulence, for example, turbulent reaction flows. In some reaction flows, the reaction scale order is much smaller than the turbulent scale order. Therefore we may truncate the reaction computation at a higher level than the turbulence computation so that the effect of the reaction will be more accurately captured.

At the end of this sub-section, let us comment upon the bubble function subspace assumption. The bubble function subspace assumption implies that the fluctuations of higher order vanish on the element boundary. This is clearly not exactly the case. A compensating method is to derive a reduced system of Eqs. (1)–(4) in the boundary surfaces of the element and then to solve it for the boundary conditions replacing the homogeneous boundary conditions of the bubble functions. Hou et al. [20,21] and Franca et al. [14] respectively used a method of this type for an elliptic problem and a diffusion – reaction problem in the multiscale finite element computations. Obviously applying this procedure in computation will increase the implementational difficulty and computational cost. Another possible approach to extend the bubble subspace is to employ discontinuous Galerkin discretization, since the discontinuous Galerkin method does not require solution continuity on the interfaces of elements, which provides more opportunity to choose the solution subspace on the element. A further investigation into the performance of these methods for LES will be carried out in our future work.

2.2. Some properties of the coefficient τ of Eq. (18)

The coefficient τ in Eq. (18) is a vector with four components to 3D flows. Its exact formulation is determined by solving the local problem (19). In order to understand its property let us explore the one-dimensional convection – diffusion problem

$$\begin{cases} \frac{\partial u}{\partial t} + a\frac{\partial u}{\partial x} - \nu\frac{\partial^2 u}{\partial x^2} = 1 \\ u(0,t) = u(h,t) = 0 \\ u(x,0) = 0 \end{cases} \tag{25}$$

The exact solution for the problem (25) can be obtained by traditional separation of variables and Fourier expansion. After solving Eq. (25) we may calculate the coefficient τ through integration on $[0,h]$. In order to simplify analysis we only consider the steady case of Eq. (25)

$$\begin{cases} a\frac{du}{dx} - \nu\frac{d^2 u}{dx^2} = 1 \\ u(0) = u(h) = 0 \end{cases} \tag{26}$$

- **When** a = 0In practical computation this case corresponds to stagnation flows. After exactly solving Eq. (26) we may calculate the coefficient τ

$$\tau = \frac{h^2}{12\nu} \tag{27}$$

From Eq. (27), it is seen that the parameter, τ, could be very large when the fluid viscosity ν is very small under fixed element diameter h. So, in order to reduce τ the element diameter h has to decrease.

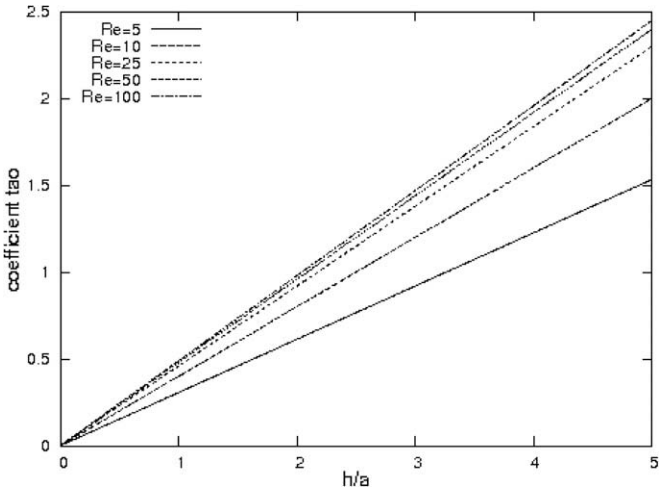

Fig. 1. Curve of τ versus $\frac{h}{a}$ for different element Reynolds numbers, Re_h.

- **When** $a \neq 0$When $a \neq 0$ the analytic solution for Eq. (26) exists and can be easily obtained,

$$y = \frac{x}{a} + \frac{h}{a\left(e^{\frac{ah}{v}} - 1\right)} - \frac{h}{a\left(e^{\frac{ah}{v}} - 1\right)} e^{\frac{ax}{v}} \tag{28}$$

After integration to the analytic solution we have

$$\tau = \frac{h}{2a} + \frac{h}{a\left(e^{\frac{ah}{v}} - 1\right)} - \frac{v}{a^2} = \frac{h}{2a} + \frac{h}{a(e^{\mathrm{Re}_h} - 1)} - \frac{h}{a\mathrm{Re}_h} \tag{29}$$

The above formula shows that the coefficient τ depends on both the ratio of the element diameter and convective velocity, $\frac{h}{a}$, and the element Reynolds number, $Re_h = \frac{ah}{v}$. Fig. 1 illustrates the τ versus $\frac{h}{a}$ curves for the different element Reynolds numbers, Re_h. We can see that in order to keep the coefficient τ constant, the mesh has to refine or the element diameter decreases when the element Reynolds number increases.

2.3. Comparison with the other similar approaches

From the above analysis we see that the small scale solution on the finest level, actually, is not exactly solved but determined in some approximation. Just because of this, the approaches of this type are viewed as a modelling of turbulence. However, it should be pointed out that the turbulence modelling of the multi-level approaches is built on a solid theoretic foundation. It gives a clear and explicit approach to accurately calculate the small scale movement, and the correlative averages of such small eddies are just the non-closed subgrid Reynolds stress in the filtered LES.

All the multi-level finite element methods have similar features. However, there are still clear differences among these approaches. They mainly lie in the way to solve the small scale movements in the subspace U^b. Certainly this is the point that distinguishes our approach from the other ones. The recent work of Bazilevs et al. [3] introduces a new general abstract formulation of multiscale finite element method for turbulence computations, which not only directly calculates the small scale movements of turbulence with the variational multiscale residual – based approach but also avoids use of eddy viscosity. One important goal of Bazilevs et al.'s work is to build an analytic solution of the small scale movements, hence they expand the small scale eddy to perturbation series with a small parameter, e.g. residual of the large eddy equations. Each term of the series requires a Green integration. In order to confine the Green operator to an element, they have to do some simplification or approximation. This work, like Bazilevs et al's work, replaces the eddy viscosity with directly calculating the small scale movements, but the major difference in algorithms between both is that we refine the element solution of the small scale eddies (Section 2.1(b)) to capture the small scale movements, which is expected to offer more accurate results for high Reynolds number flows or high Peclet number convections.

Recently, in the finite volume community, the implicit LES have been actively studied, see [1,4,19,28,36]. The implicit LES approach does not explicitly calculate the subgrid Reynolds stress but determines them from transferring the truncation error of the discrete equations. The basic idea may be simply explained thus: when the exact solution of the problem is

substituted into the discrete Navier–Stokes equations without the subgrid Reynolds stress, the discrete equation does not hold due to the truncation error. The subgrid Reynolds stress should play a role such as to make the exact solution satisfy the discrete equations when it is embedded. One may see that our approach has the similar idea to the implicit LES of the finite volume method although our implementation is different from them.

3. Implementation

Solving the problem (18) by the finite element method is straightforward and can be carried out by standard procedures. The only additional work is to calculate the parameter τ and to assemble the additional terms associated with it while assembling each element matrix. In order to calculate the parameter τ or small scale movements we need to solve the problem (19) or (15). Note that the problem (19) equals the problem (15) normalised by the residual of Eq. (18). This section will address a spectral – element solution for it.

The computational domain of Eq. (19) is an element of mesh. It is known that a tetrahedral element is a basic element in unstructured meshes. Any elements of other types may be decomposed into the combinations of tetrahedral elements. Therefore we only consider the solution of Eq. (19) on a tetrahedral element. By element split, the method for tetrahedral element can be easily extended to element of any other type. The variational formation for problem (19) on one element reads

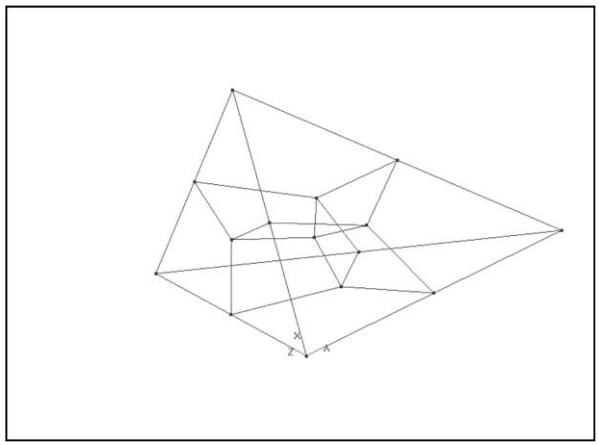

Fig. 2. One tetrahedral is split into four hexahedrons.

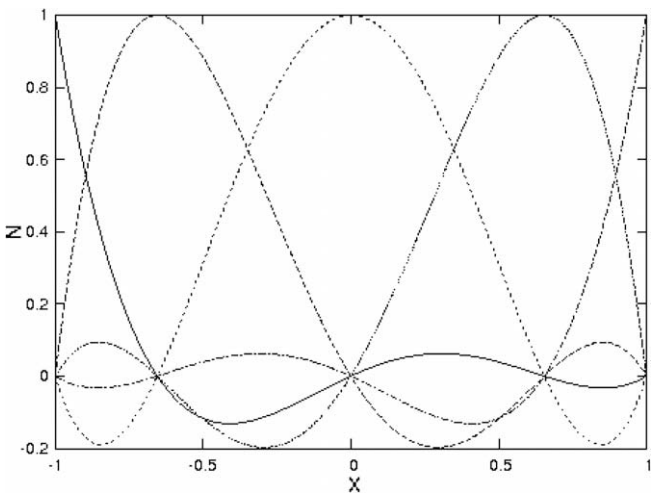

Fig. 3. Five Lagrangian interpolation polynomials of order four.

$$(L(S^b), v^b) + \tau_{e\_b}((L(S^b) - 1), L^*(v^b)) = (1, v^b) \tag{30}$$

where $S^b \in U_n^h$ and $v^b \in U_n^h$, and U_n^h is the set of n – order polynomials defined in the element E that will be given in (32). The parameter τ_{e_b} has the same form as mentioned in Section 2.1(a) but a different sub-element diameter. In order to implement a spectral element method on a tetrahedral element we spatially decompose the tetrahedral element into four hexahedral elements, see Fig. 2. The solution S^b within each hexahedral element is expanded to

$$S^b = \sum_{i,j,k=0}^{n} N_i(\xi)N_j(\eta)N_k(\varsigma)s(t) \tag{31}$$

where $-1 \leqslant \xi,\eta,\varsigma \leqslant 1$ are the local coordinate of the reference cube that the hexahedral element is mapped to. The shape function $N(\chi)$ is defined by Lagrangian interpolation

$$N_i(\chi) = -\frac{(1-\chi^2)P_n'(\chi)}{n(n+1)P_n(\chi_i)(\chi - \chi_i)} \tag{32}$$

where $P_n(\chi)$ is a Legendre polynomial of degree n and χ_i denotes the ith Gauss– Lobatto–Legendre (GLL) point that is given by the root of

$$(1-\chi^2)P_n'(\chi) = 0 \tag{33}$$

Fig. 3 illustrates the Lagrangian interpolation polynomials for $n = 4$. We see the element nodes localise at the quadrature points that attach the discrete solutions in the element. Two relationships for the Lagrangian interpolation polynomials and its derivative are essential for implementation of the algorithm, which comes from [7]

$$N_i(\chi_j) = \begin{cases} 1, & i = j \\ 0, & i \neq j \end{cases} \tag{34}$$

$$\frac{\partial}{\partial\chi}[N_i(\chi_j)] = \begin{cases} \frac{P_n(\chi_j)}{P_n(\chi_i)}\frac{1}{\chi_j - \chi_i}, & i \neq j \\ -\frac{n(n+1)}{4}, & i = j = 0 \\ \frac{n(n+1)}{4}, & i = j = n \\ 0, & \text{otherwise} \end{cases} \tag{35}$$

Substituting (31) into (30) and doing the inner integrations of each term of (30), we have following semi-discrete equations:

$$\frac{ds(t)}{dt} = Ms(t) + R \tag{36}$$

where M is the stiffness matrix and R the source term coming from the upper-level residual. When assembling Eq. (34) we need to know the effect of the higher level's movements on this level's, i.e., the coefficient τ_{e_b} in the variational formulation (30). This coefficient is obtained by Eq. (20) or (21) or (22) with the refined element diameter. Eq. (34) is integrated by the implicit second order trapezoidal scheme. Hence the major computational workload is to solve a set of linear equation system, which is calculated by LU decomposition in this work.

Let us explain a little more about treatment of the BCs during assembly of the matrixes. Due to the Dirichlet Boundary conditions in the problem (19), $s(t)$ must be known at one node, which is on the element edges, of the two boundary nodes of the nodal stencil and the other boundary node (inner boundary node of this stencil) must link with the inner boundary node(s) of the nodal stencil of the other hexahedral element. Because of requirement for continuity of the solution, $s(t)$ at the common nodes must be equal. This condition couples all the equations of the four sub-elements. The number of degrees of freedom (DOF) for each unknown variable can be calculated by 4 (number of the split hexahedral elements) $\times n^3$ (orders of the Lagrangian interpolation – number of boundary conditions, $(n+1)-1$, to 3 spatial dimensions) $-\{6\times(n-1)^2 + 4\times 2\times(n-1) + 3\times 1\}$ (number of inner boundary conditions), or another equivalent formula for that, $4\times(n-1)^3 + 6\times(n-1)^2 + 4\times(n-1) + 1$.

In summary, the whole calculation procedure can be described as follows

```
Start initial state for t = 0
  For t = t + Δt
    Newton iteration
      Solve (34)
      Calculate τ of (18) from integral of solution of (34)
      Assemble matrix for (18)
      Solve discrete equations of (18)
    End Newton iteration
    Update solution
  Do next time step
End
```

Implementing the above program we used UG software, see [2].

Table 1
Degree of freedom for the spectral finite element methods.

Method	Tetrahedral element	Hexahedral element
Third order	65	8
Fourth order	175	27
Fifth order	369	64
Sixth order	671	125

Table 2
Tested velocities and pressure.

	U	V	W	P
Case 1	0	0	0	0
Case 2	1	0	0	0
Case 3	0.57735	0.57735	0.57735	0

Table 3
Coefficient τ at fixed element Reynolds number $Re^e = 5$ and element diameter $h = 0.1$.

Method	Case 1	Case 2	Case 3
Third order	0.00940, 0.00940 0.00940, 0	0.00305, 0.00284 0.00284, −0.00093	0.00315, 0.00315 0.00315, −0.00163
Fourth order	0.00981, 0.00981 0.00981, 0	0.00329, 0.00301 0.00301, −0.00096	0.00335, 0.00335 0.00335, −0.00166
Fifth order	0.00986, 0.00986 0.00986, 0	0.00645, 0.00559 0.00559, −0.00203	0.00651, 0.00651 0.00651, −0.00356
Sixth order	0.00986, 0.00986 0.00986, 0	0.00646, 0.00560 0.00560, −0.00204	0.00652, 0.00652 0.00652, −0.00356

Table 4
Coefficient τ at fixed element Reynolds number $Re^e = 100$ and element diameter $h = 0.1$.

Method	Case 1	Case 2	Case 3
Third order	0.188, 0.188 0.188, 0	0.00440, 0.00398 0.00398, −0.00132	0.00468, 0.00468 0.00468, −0.00233
Fourth order	0.196, 0.196 0.196, 0	0.00494, 0.00432 0.00432, −0.00138	0.00514, 0.00514 0.00514, −0.00239
Fifth order	0.197, 0.197 0.197, 0	0.0159, 0.0128 0.0128, −0.00372	0.0163, 0.0163 0.0163, −0.00714
Sixth order	0.197, 0.197 0.197, 0	0.0162, 0.0130 0.0130, −0.00376	0.0166, 0.0166 0.0166, −0.0075

Table 5
Coefficient τ at fixed element Reynolds number $Re^e = 5$ and element diameter $h = 1$.

Method	Case 1	Case 2	Case 3
Third order	0.940, 0.940 0.940, 0	0.043, 0.039 0.039, −0.0129	0.0456, 0.0456 0.0456, −0.0228
Fourth order	0.981, 0.981 0.981, 0	0.0481, 0.0422 0.0422, −0.0135	0.05, 0.05 0.05, −0.0233
Fifth order	0.985, 0.985 0.985, 0	0.148, 0.118 0.118, −0.037	0.152, 0.152 0.152, −0.0702
Sixth order	0.986, 0.986 0.986, 0	0.1496, 0.1199 0.1199, −0.0368	0.153, 0.153 0.153, −0.0707

According to the above algorithm, for each refined element it is required to solve Eq. (34) once for each Newton iteration. The computational cost for that mainly depends on the number of DOF of (34). In order to find the least DOF, we investigate the parameter$\tau$by solving Eq. (34) on one hexahedral element for different cases. First of all we tabulate the DOF for tetra-

Table 6
Coefficient τ at fixed element Reynolds number $Re^e = 100$ and element diameter $h = 1$.

Method	Case 1	Case 2	Case 3
Third order	18.8, 18.8 18.8, 0	0.0450, 0.0406 0.0406, −0.0134	0.0479, 0.0479 0.0479, −0.024
Fourth order	19.6, 19.6 19.6, 0	0.05066, 0.0441 0.0441, −0.01414	0.0529, 0.0529 0.0529, −0.0244
Fifth order	19.7, 19.7 19.7, 0	0.171, 0.139 0.139, −0.036	0.173, 0.173 0.173, −0.0694
Sixth order	19.7, 19.7 19.7, 0	0.1778, 0.1432 0.1432, −0.038	0.1823, 0.1823 0.1823, −0.083

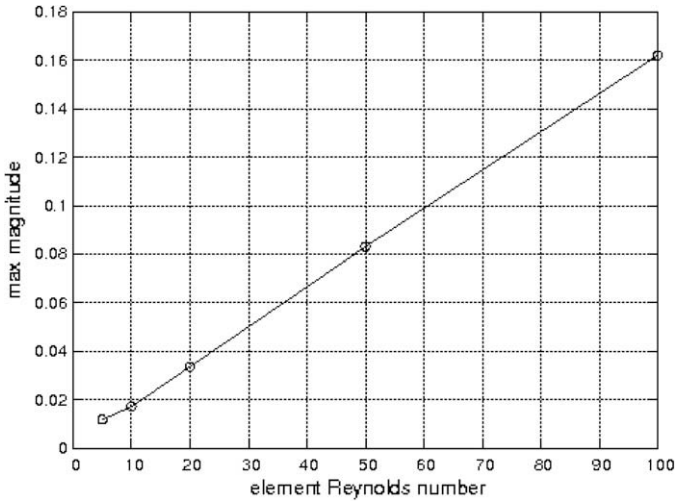

Fig. 4. Maximum magnitude of the small scale movements versus element Reynolds numbers.

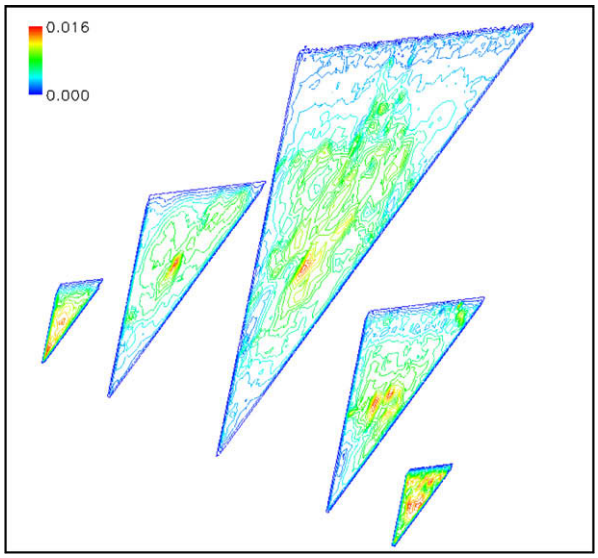

Fig. 5. Distribution of iso-magnitude of the small scale eddies on 5 cross-sections of tetrahedron at $Re^e = 100$.

hedral and hexahedral elements in Table 1. It may be seen that the DOF of tetrahedral element is not four times but approximately six times ones of hexahedral element. This is because the variables at the inner common boundary nodes of the hexagonal elements split from the tetrahedral element are unknown and so it produces the additional DOF.

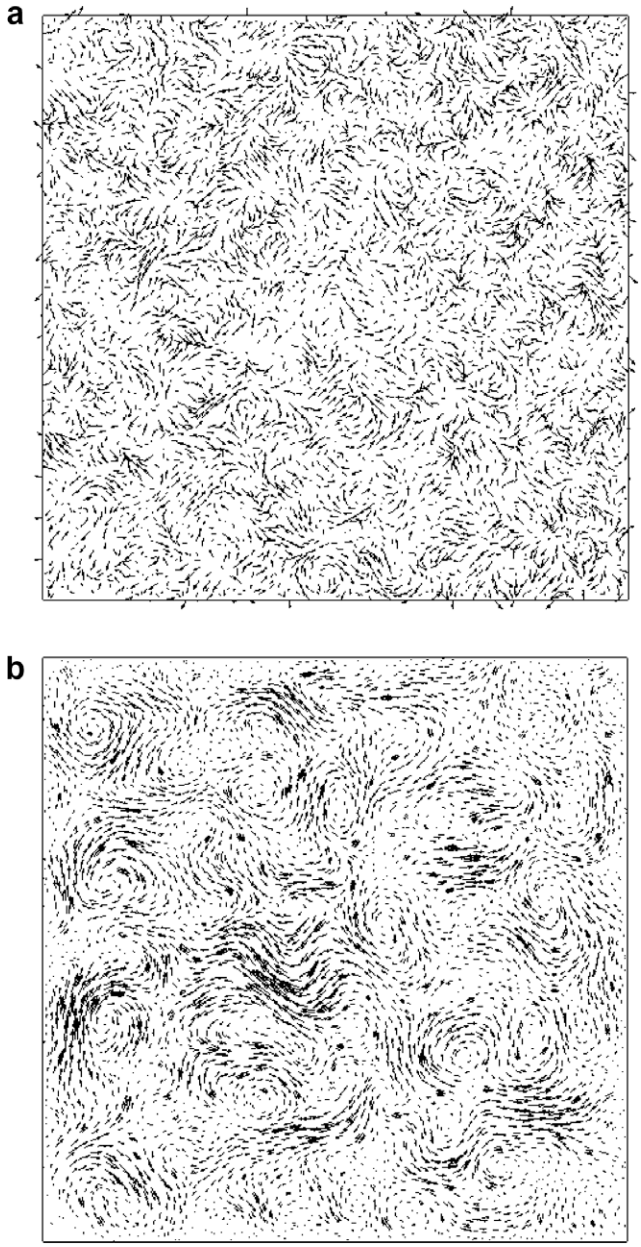

Fig. 6. Comparison of two cross-section velocity vectors: (a) inlet section and (b) middle section.

The three typical cases are calculated in which constant velocities and pressure are taken as the flow states of the upper level, see Table 2.

The computational domain is a cubic element with the edge h.[3] From the analysis of Section 2.2 we know that the coefficient τ generally depends on not only the ratio of the element diameter and convective velocity but also the element Reynolds number. We particularly take four sets of cases, $(Re^e,h) = (5, 0.1)$, $(Re^e,h) = (100, 0.1)$, $(Re^e,h) = (5, 1)$ and $(Re^e,h) = (100, 1)$ for calculating the coefficientτ. The results are listed in Tables 3–6. From the computational results we found that the fifth and sixth order methods give nearly same coefficients and significantly differs ones by the third and fourth order methods. They appear not to depend on the element Reynolds number and element diameter in our tested cases, except for Table 4. This suggests that the least DOF is 64 in the tested element Reynolds number scope.

[3] It should be pointed out that we also did many irregular element calculations and found that almost invariably the shape of element does not affect the computational results.

4. Numerical tests

In this section, three numerical computations are presented, in order to investigate the properties and behaviour of the introduced numerical scheme. They are the small scale eddy simulation in a tetrahedral element, homogeneous decaying turbulence and circular pipe turbulence.

4.1. The small scale eddy simulation in a tetrahedral element

The first numerical test is a numerical simulation of small scale movements in a tetrahedral element, in which we numerically solve Eq. (19) in a tetrahedral element. The purpose of this case study is to explore the detailed structure of the small scale eddies within the tetrahedral element described by Eq. (19). In the traditional LES, these small scale eddies are not calculated but are modelled as subgrid Reynolds stresses acting on the calculated large eddies.

It is reminded that a real small scale movement in an element is obtained by solving Eq. (15). It can be found from Eq. (15) that the small scale movement depends on the residual from the upper level, i.e., it is as a source to drive the small scale movement. If the residual equals zero, there is no small scale movement any more on this level, since the "exact" solution is already obtained on the upper level. In order to character the small scale movement, a normalization of Eq. (15) using a

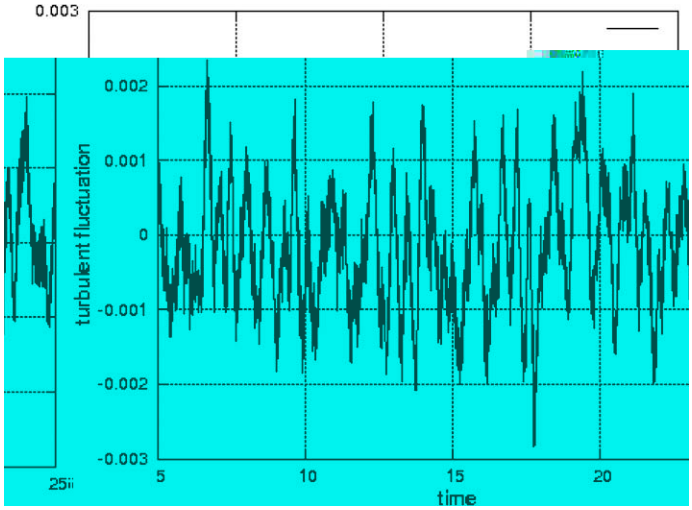

Fig. 7. Turbulent fluctuation in time domain at central location.

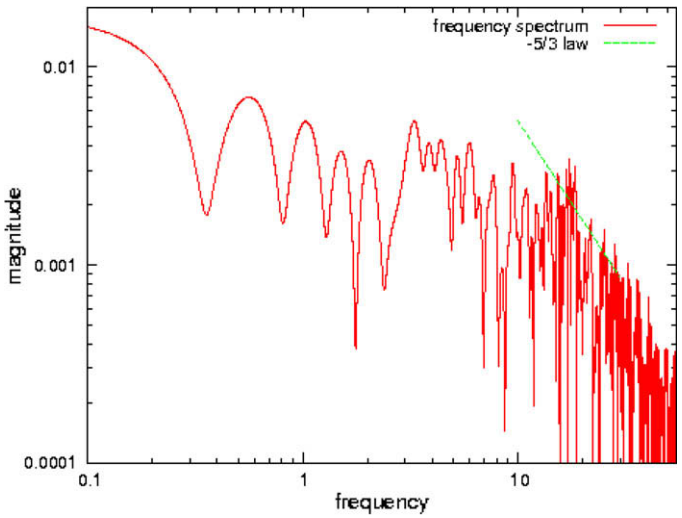

Fig. 8. Turbulent energy spectrum of Fig. 8 and its comparison with −5/3 law.

norm of the residual gives Eq. (19). After solving Eq. (19), we may get the real small scale movements by multiplying a factor (the norm). In this numerical test, we just solve Eq. (19) for a general investigation of the small scale movement features.

We investigated five cases with different Reynolds numbers, Re^e = 5, 10, 20, 50 and 100. In all the computations we took the averaged flow velocity from large eddies as a constant, $(-0.5,-0.5,-0.5)$. The computational domain is a tetrahedral element with vertexes (0,0,0), (1,0,0), (0.5,1,0) and (0.5,0.5,1). This tetrahedron is meshed by about 220,000 tetrahedral elements. The element Reynolds number in the computations will not exceed 2. Therefore, all the computations in this case study were carried out with Eq. (21) rather than solving the spectral-element problem. For each computation we integrated the time to 5 unit.

The variation of maximum magnitude of the small scale movements versus the Reynolds numbers, Re^e, is shown in Fig. 4. It is apparent that the maximum value increases linearly with element Reynolds number. When Re^e=100, there is obvious scale-separated movements. The maximum magnitude of the small scale eddies exceeds 20% of the averaged large eddy magnitude. Fig. 5 illustrates the distribution of iso-magnitude of the small eddies on five cross-sections of the tetrahedron at Re^e = 100. It is observed that most of the eddies are of a magnitude order one-tenth of the maximum magnitude of the small scale eddies. This observation suggests that for a large element Reynolds number, it is necessary to adopt two ways to represent the small scale eddies: one is the spectral-element approximation for the larger scale part and the other is for the smaller scale part, e.g. using Eqs. (20),(21), or (23).

4.2. Homogenous decaying turbulence

The second computed case is a decaying homogenous turbulence. The flow is characterised by an uniform averaged velocity field in a domain, $x \times y \times z = 1 \times 1 \times 2$ (z is the stream-wise direction), which is set up with an uniform averaged velocity $\begin{cases} u = 0 \\ v = 0 \\ w = 1 \end{cases}$ on the inlet boundary and a mixing combination, $\begin{cases} \frac{\partial u}{\partial n} = 0 \\ \frac{\partial v}{\partial n} = 0 \\ w = 1 \end{cases}$, for the side boundary conditions. The free boundary condition is specified for the outlet boundary. Because of the uniform averaged flow field, turbulence will not be produced, thus the disturbances introduced in the inlet flow will decay. Theory found that the turbulent energy spectrum in a homogenous turbulence satisfies a $-5/3$ decay law with respect to the frequency [34]. In order to generate the homogenous turbulence, we enforce a fluctuation on the inlet boundary conditions:

$$\begin{cases} u' = 0.01 \ \sin[2\pi \times random(t)] \\ v' = 0.01 \ \sin[2\pi \times random(t)] \\ w' = 0.01 \ \sin[2\pi \times random(t)] \end{cases} \tag{37}$$

where random (t) is a random function and its spectrum has a rectangle distribution. The sine function restricts the random function values from -1 to 1. A correct numerical simulation for this turbulence should give a turbulent energy spectrum decay with $-5/3$ law, as predicted by the theory.

The computational domain is meshed by about 750,000 tetrahedral elements that are uniformly distributed in the computational domain and the Reynolds number is 10,000. A third order method of spectral element is applied to calculate the second level flows in each tetrahedral element. The initial flow state is static. The integral time step width is 0.02s and 5000 time steps are integrated, therefore the time interval is 100s.

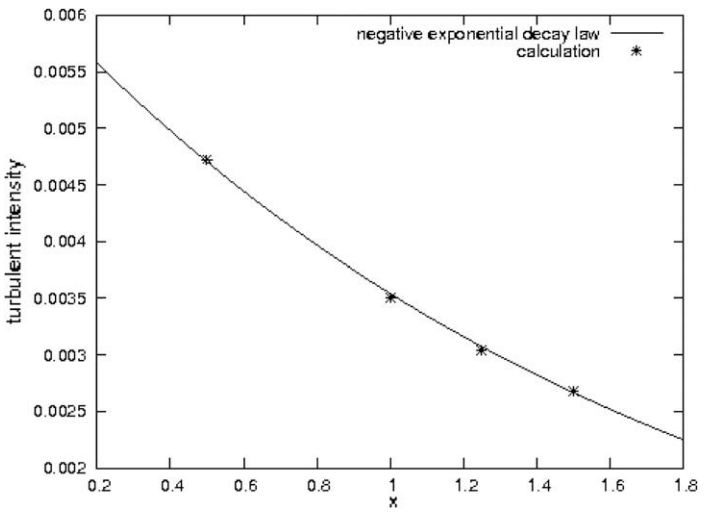

Fig. 9. Turbulence intensity decay along central line that is fitted with the negative exponential decay lay.

Fig. 6 shows turbulent fluctuations on two cross-sections, one is the inlet section and the other is the cross-section at $z = 1$ location. It may be seen that the fluctuation on the inlet is completely random, but with its development, a clear and coherent vortex structure is generated, see (b) of Fig. 6. This is a substantial feature of turbulence. We also sampled the velocity fluctuations at four locations, $z = 0.5$, $z = 1.0$, $z = 1.25$ and $z = 1.5$ at $x = 0.5$ and $y = 0.5$. A typical turbulent fluctuation in the time domain is shown in Fig. 7 (at $z = 1.5$). The discrete Fourier transform to it will give the energy spectrum. 3500 sample data points, from 1000th to 4500th, are used for the discrete Fourier transform. The Fourier transform upper limit is 1,048,576. The energy spectrum is shown in Fig. 8 and for comparison the $-5/3$ law is also drawn in Fig. 8. It may be seen that it decays in agreement with $-5/3$ law. Further if we fit the turbulent intensity at the four sampled points using an exponential function, then it is found to satisfy a negative exponential decay law, see Fig. 9.

4.3. Circular pipe turbulence

Circular pipe turbulence is a classical turbulent flow. Historically Reynolds firstly found turbulence in a pipe flow. Much theoretical, numerical and experimental research has been published, e.g. see [11,29,34,37]. We calculated it to check our

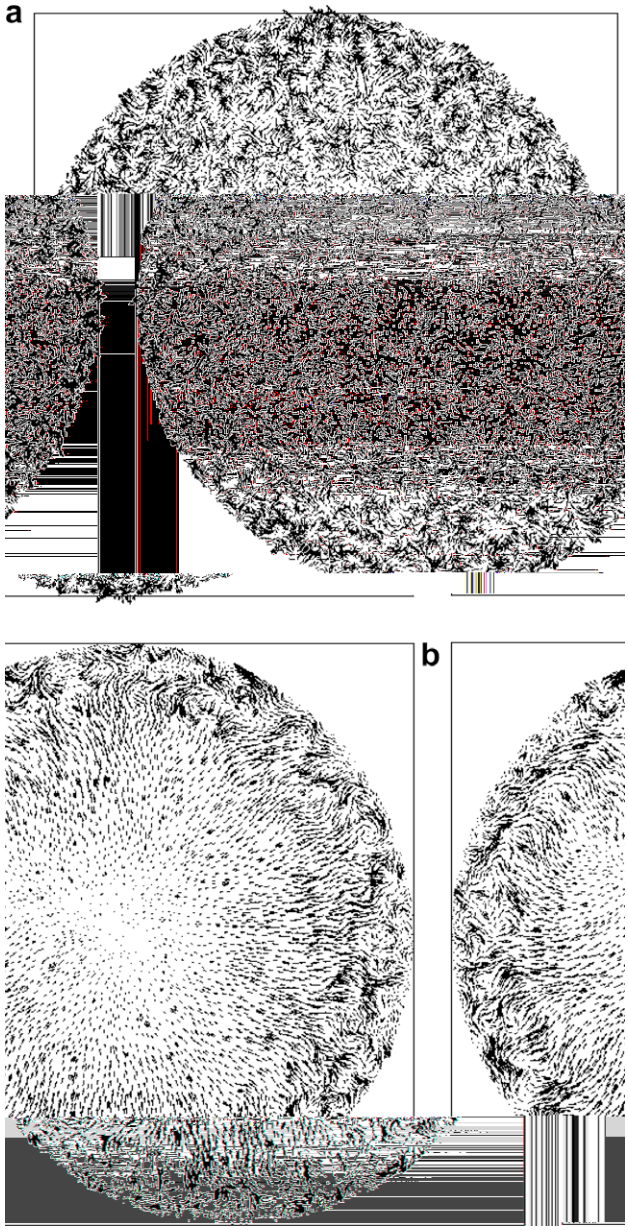

Fig. 10. Velocity vector projections on inlet and middle cross-sections: (a) inlet section and (b) middle section.

numerical method. A length of circular pipe, 7.5 diameters long, is taken as the computational domain which is meshed by about 860,000 tetrahedral elements. The elements are non-informally distributed in the computational domain, and the closer to the wall the grater the number of elements. One end of the pipe is the inlet and the other outlet. In the inlet we impose a prescribed mean velocity and random fluctuations which simulates real turbulence on the section

$$\begin{cases} u = 0.01\left[0.5 + \left(\frac{r}{R}\right)^2\right]\sin[2\pi \times \ \text{random}(t)] \\ v = 0.01\left[0.5 + \left(\frac{r}{R}\right)^2\right]\sin[2\pi \times \ \text{random}(t)] \\ w = \left(1 - \frac{r}{R}\right)^{0.15} + 0.01\left[0.5 + \left(\frac{r}{R}\right)^2\right]\sin[2\pi \times \mathit{random}(t)] \end{cases} \tag{38}$$

where random(t) is a random function and, the sine function restricts the random function values from -1 to 1. The output boundary condition is free, described in Eq. (4). The wall of the pipe has a no-slip condition. The Reynolds number is 10,000, which is based on the inlet bulk velocity, pipe diameter and viscosity of fluid. The third order method of spectral element is applied to calculate the second level flows in a tetrahedral element. The calculation is terminated when time = 250 s (5000×0.05).

The flow velocity vectors projected on two cross-sections of the pipe are drawn in Fig. 10, one is the inlet section and the other is located in the middle of the pipe. Comparing the figures, it may be seen that the fluctuations in the central area of the pipe rapidly decay and a kind of coherent eddy structures settles in the near-wall region. These coherent eddies, in fact,

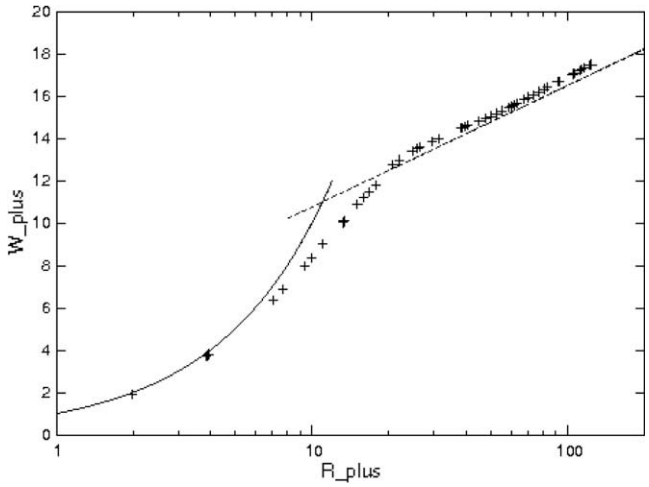

Fig. 11. Calculated mean velocity comparison with the wall law.

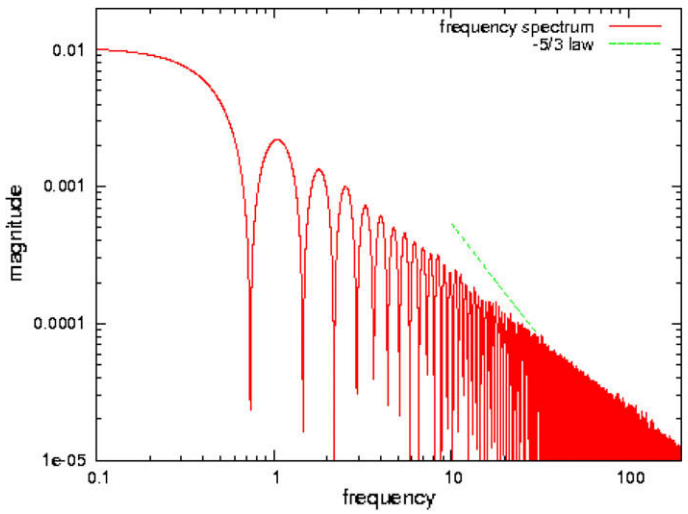

Fig. 12. Turbulent energy spectrum at 0.9 radius location and its comparison with $-5/3$ law.

maintain the production of major turbulence in the pipe flow and lead to a high fluctuation near the wall. The results obtained by our computation are in agreement with previous numerical simulations and experiments, see [37].

For a pipe flow with Reynolds number 10,000, its friction factor is $f = 3.14 \times 10^{-2}$ [29]. We, therefore, can obtain the friction velocity by $f = 8\frac{u_\tau}{V_{bulk}}$. The calculated mean velocity profile is illustrated on Fig. 11 in wall units. The mean axis velocity is calculated through by 10 cross-section velocity distributions from $z = 10$R (R is radius of the pipe) to 14.5 R. A comparison with the wall law is displayed in Fig. 11. It is apparent that the computed results are basically in agreement with the wall law but slightly over-predicts in the pipe core region.

The turbulent energy spectrum at $r = 0.9$ R and $z = 10$ R is shown in Fig. 12. We recorded 5000 velocity fluctuation samples at that point, and 3500 sample data, from 1000th to 4500th, were used to calculate the mean value and discrete Fourier transform. The upper Fourier transform limit is taken as 1,048,576. In Fig. 12 the $-5/3$ law is also plotted for comparison. It can be seen that the fluctuation energy spectrum decays according to a power function rule and its index is slightly greater than $-5/3$. The reasons for this could have arisen either from two ways: one is that the calculated pipe Reynolds number is not high enough and the other is that the sampled fluctuations in the near wall region is not in an ideal inertial subrange.

5. Conclusions

In this work we introduce a hierarchical formulation of finite element for LES. The hierarchical formulation is applied to a three-level case, for which we devised a triple-level method. The first level is solved by the conventional finite element method, the second level by a spectral element method and the last level is simulated by the analytic formulae that come from the stabilised finite element method. This method affords an numerical approach toward explicityly and accurately calculating turbulence, exactly, the effect of the small scale eddies on the large scale eddies is directly calculated so as to avoid the unclosed problem of the traditional LES.

The whole numerical method is designed for unstructured meshes, and therefore may be applied to turbulence simulations for complex geometries. The numerical tests show that the degree of freedom for the second level calculation should exceed 64 in order to accurately capture the small scale eddies. The introduced method was applied to calculate a homogenous decaying turbulence and circular pipe turbulence and produced the reasonable results.

Acknowledgement

I would like to thank the two anonymous reviewers whose comments much helped to improve the clarity of the paper.

References

[1] N.A. Adams, S. Hickel, S. Franz, Implicit subgrid-scale modelling by adaptive deconvolution, J. Comput. Phys. 200 (2004) 412–431.
[2] P. Bastian, K. Birken, K. Johannsen, S. Lang, N. Neuss, H. Rentz-Reichert, C. Wieners, UG-a flexible software toolbox for solving partial differential equations, Comput. Visual. Sci. 1 (1997) 27–40.
[3] Y. Bazilevs, V.M. Calo, J.A. Cottrell, T.J.R. Hughes, A. Reali, G. Scovazzi, Variational multiscale residual-based turbulence modelling for large eddy simulation of incompressible flows, Comput. Meth. Appl. Mech. Eng. 197 (2007) 173–201.
[4] J.P. Boris, F.F. Grinstein, E.S. Oran, R.J. Kolbe, New insights into large eddy simulation, Fluid Dyn. Res. 10 (1992) 199–228.
[5] F. Brezzi, D. Marini, A. Russo, Applications of the pseudo residual-free bubbles to the stabilization of convection-diffusion problems, Comput. Meth. Appl. Mech. Eng. 166 (1998) 51–63.
[6] C. Calgaro, J. Laminie, R. Teman, Dynamical multilevel schemes for the solution of evolution equations by hierarchical finite element discretization, Appl. Numer. Math. 23 (1997) 403–442.
[7] C. Canuto, M.Y. Hussaini, A. Quarteroni, T.A. Zang, Spectral Methods in Fluid Dynamics, Springer–Verlag, Heidelberg, New York, 1988.
[8] R. Codina, A stabilised finite element approximation of transient incompressible flows using orthogonal subscale, Comput. Meth. Appl. Mech. Eng. 191 (2002) 4295–4321.
[9] S.S. Collis, Monitoring unresolved scale in multiscale turbulence modelling, Phys. Fluids 13 (6) (2001) 1800–1806.
[10] J.A. Domaradzki, E.M. Saiki, A subgrid-scale model based on the estimation of unresolved scale of turbulence, Phys. Fluids 9 (7) (1997) 2148–2164.
[11] F. Durst, J. Jovanovic, J. Sender, LDA measurements in the near-wall region of a turbulent pipe flow, J. Fluid Mech. 295 (1995) 305–335.
[12] C. Foias, G.R. Sell, R. Teman, Inertial manifolds for nonlinear evolutionary equations, J. Differ. Equations 73 (1988) 309–353.
[13] C. Foias, M.S. Jolly, I.G. Kevrekidis, G.R. Sell, E.S. Titi, On the computation of inertial manifolds, Phys. Lett. A 131 (1988) 433–436.
[14] L.P. Franca, L.M. Alexandre, F. Valentin, Towards multiscale functions: enriching finite element space with local but not bubble-like functions, Comput. Meth. Appl. Mech. Eng. 194 (2005) 3006–3021.
[15] L.P. Franca, S.L. Frey, Stabilised finite element methods: II. The incompressible Navier–Stokes equations, Comput. Meth. Appl. Mech. Eng. 99 (1992) 209–233.
[16] V. Gravemeier, W.A. Wall, E. Ramm, A three-level finite element method for the instationary incompressible Navier–Stokes equations, Comput. Meth. Appl. Mech. Eng. 193 (2004) 1323–1366.
[17] V. Gravemeier, Scale-separating operators for variational multiscale large eddy simulation of turbulence flows, J. Comput. Phys. 212 (2006) 400–435.
[18] V. Gravemeier, A.W. Wolfgang, E. Ramm, Large eddy simulation of turbulent incompressible flows by a three-level finite element method, Int. J. Numer. Meth. Fluids 48 (2005) 1067–1099.
[19] S. Hickel, N.A. Adams, J.A. Domaradzki, An adaptive local deconvoltion method for implicit LES, J. Comput. Phys. 213 (2006) 413–436.
[20] T.Y. Hou, X.H. Wu, A multiscale finite element method for elliptic problems in composite materials and porpous media, J. Comput. Phys. 134 (1997) 169–189.
[21] T.Y. Hou, X.H. Wu, Z. Cai, Convergence of a multiscale finite element method for elliptic problems with rapidly oscillating coefficients, Math. Comput. 68 (227) (1999) 913–943.
[22] T.J.R. Hughes, Multiscale phenomena: Green's functions, the Dirichlet-to-Neumann formulation, subgrid scale models, bubbles and the origins of stabilised methods, Comput. Meth. Appl. Mech. Eng. 127 (1995) 387–401.
[23] T.J.R. Hughes, A.A. Mazzei, K.E. Jansen, large-eddy simulation and the variational multiscale method, Comput. Visual. Sci. 3 (2000) 47–59.

[24] T.J.R. Hughes, G. Sangalli, Variational multiscale analysis: the finescale Green's function, projection, optimization, localisation and stabilised methods, SIAM J. Numer. Anal. 45 (2007) 539–557.
[25] B. Knaepen, O. Debliquy, D. Carati, Large-eddy simulation without filter, J. Comput. Phys. 205 (1) (2005) 98–107.
[26] W. Liu, Modeling of Swirling Turbulent Flows, IHS-Mitteilungen, vol. 22, Stuttgart University, 2001.
[27] W. Liu, G. Makhviladze, An implicit finite element solution of thermal flows at low Mach number, J. Comput. Phys. 227 (2008) 2743–2757.
[28] L.G. Margolin, W.J. Rider, F.F. Grinstein, Modelling turbulent flow with implicit LES, J. Turbulence 7 (2006) 1–27.
[29] B.J. McKeon, C.J. Swanson, M.V. Zagarola, R.J. Donnelly, A.J. Smits, Friction factors for smooth pipe flow, J. Fluid Mech. 511 (2004) 41–44.
[30] E.A. Munts, S.J. Hulshoff, R.de. Borst, A model-based multiscale method for large eddy simulation, J. Comput. Phys. 224 (2007) 389–402.
[31] J. Smagorinsky, Some historical remarks on the use of nonlinear viscosities, in: B. Galperin, S.A. Orszag (Eds.), Large Eddy Simulation of Complex Engineering and Geophysical Flows, Cambridge University Press, Cambridge, 1993, pp. 3–36.
[32] R. Teman, Inertial manifolds and multigrid methods, SIAM J. Math. Anal. 21 (1990) 154–178.
[33] R. Teman, Multilevel method for the simulation of turbulence, a simple model, J. Comput. Phys. 127 (1996) 309–315.
[34] H. Tennekes, J.L. Lumley, A First Course in Turbulence, The MIT Press, 1972.
[35] T.E. Tezduyar, S. Mittal, S.E. Ray, R. Shih, Incompressible flow computations with stabilised bilinear and linear equal-order-interpolation velocity-pressure elements, Comput. Meth. Appl. Mech. Eng. 95 (1992) 221–242.
[36] B. Thornber, A. Mosedale, D. Drikakis, On the implicit large eddy simulations of homogeneous decaying turbulence, J. Comput. Phys. 226 (2007) 1902–1929.
[37] X. Wu, P. Moin, A direct numerical simulation study on the mean velocity characteristics in turbulent pipe flow, J. Fluid Mech. 608 (2008) 81–112.